H_∞ robust control design of active structural vibration suppression using an active mass damper

Smart Mater. Struct. **17** (2008) 015021 (10pp) doi:10.1088/0964-1726/17/01/015021

H_∞ robust control design of active structural vibration suppression using an active mass damper

Linsheng Huo[1,2], Gangbing Song[2,3], Hongnan Li[1] and Karolos Grigoriadis[2]

[1] School of Civil and Hydraulic Engineering, Dalian University of Technology, Dalian 116024, People's Republic of China
[2] Department of Mechanical Engineering, University of Houston, Houston, TX 77204, USA

E-mail: gsong@uh.edu

Received 21 June 2007
Published 11 December 2007
Online at stacks.iop.org/SMS/17/015021

Abstract

A mathematical model of any real system is always just an approximation of the true, physical reality of the system dynamics. There are always uncertainties in the system modeling. This paper outlines a general approach to the design of an H_∞ control of an active mass damper (AMD) for vibration reduction of a building with mass and stiffness uncertainties. Linear fractional transformation (LFT) is utilized in this paper for uncertainty modeling. To facilitate the computation of the H_∞ controller, an efficient solution procedure based on linear matrix inequalities (LMIs) is employed. The controller uses the acceleration signal for feedback. A two-story building test-bed with an AMD is used to test the designed H_∞ controller. Earthquake ground motion is introduced by a shaking table. A pair of diagonal shape memory alloy (SMA) wire braces are installed in the first floor to introduce stiffness uncertainty to the structure by controlling the temperature of the SMA wire brace. Masses are added to the structure to introduce mass uncertainty. Experiments were conducted and the results validate the effectiveness of the proposed H_∞ controller in dealing with stiffness and mass uncertainties.

(Some figures in this article are in colour only in the electronic version)

1. Introduction

Civil engineering structures located in areas where earthquakes or large wind forces are common are subjected to serious structural vibrations during their lifetime. The level of these vibrations can range from harmless to severe, with the latter possibly resulting in serious structural damage and potential structural failure. Even though engineers cannot design a building that is damage-proof during earthquakes and strong winds, the approach of structural control is promising in reducing the vibration of structures. A structural control device is defined as an electro-mechanical system that is installed in a structure to reduce structural vibrations in various loading scenarios, such as strong winds and earthquakes. The purpose of such a structural control system is to enhance the safety as well as improve the habitability of structures during these events. A structural control system is commonly classified by its device type, which results in three general types: passive, active and semi-active. Active control systems have the ability to adapt to different loading conditions and to control vibration modes of the structure (Housner *et al* 1997). The most commonly investigated active control devices are active mass dampers (AMDs), which were developed by introducing an active controlled actuator in a tuned mass damper (TMD). In 1989, the Kyobashi Seiwa Building in Tokyo, Japan, was constructed using an AMD, making it the first building in the world to use an active structure (Kobori *et al* 1991). However, there are important issues that remain to be addressed in the area of AMD structural control, such as system instability due to structural modeling errors.

A civil engineering structure is a continuum with an infinite number of degrees of freedom. Its system parameters

[3] Author to whom any correspondence should be addressed.

may vary under large external loadings. Therefore, it is important that a controller possess robustness to various system parameter variations and uncertainties. Robust control focuses on the issues of the performance and the stability of the closed-loop system in the presence of uncertainty, both in the parameters of the system and in exogenous inputs. The H_∞ approach is advantageous since it can address both attenuation of disturbances and perturbation of parameters (Chen and Patton 1999). The H_∞ optimal robust control technique is used in this paper for vibration suppression of building structures.

Doyle *et al* (1989) developed state–space formulas for all controllers that solve a standard H_∞ problem, thereby making a significant breakthrough in H_∞ control. H_∞ design methods may be found in many references, such as Kwakernaak (1993), Doyle *et al* (1989), Wang *et al*, (1995a, 1995b, 1998), and Zhou *et al* (1996). H_∞ control methods provide controllers with robustness to external disturbances and system parameter uncertainty, such as modeling errors and system parameter perturbations. Therefore, these controllers can guarantee stability and optimized vibration suppression performance despite insufficient or inaccurate knowledge of the structural system parameters. Recent formulations of the H_∞ control problem in terms of linear matrix inequality (LMI) allow computationally efficient and systematic design of robust controllers (Skelton *et al* 1998).

This paper presents the application of the H_∞ control theory to designing controllers for structures with AMDs, taking into account mass and stiffness uncertainties. For synthesizing the H_∞ controller, we use a linear matrix inequality (LMI) formulation (Iwasaki and Skelton 1994, Gahinet and Apkarian 1994). More precisely, the H_∞ control problem can be formulated as a minimization problem subject to convex constraints expressed by a system of LMIs. The control design method is tested on an AMD vibration control experiment. The controller uses the acceleration signal for feedback. A two-story building test-bed with an AMD is used to test the designed H_∞ controller on a shaking table. To study the robustness of the H_∞ controller, a pair of diagonal shape memory alloy (SMA) wire braces are installed in the first floor to introduce stiffness uncertainties to the structure by controlling the temperature of the SMA braces. Masses are added to the structure to introduce mass uncertainties. Experiments are conducted to validate the effectiveness of the proposed H_∞ controller in dealing with both stiffness and mass uncertainties.

2. Dynamics of the control system with an AMD

A structural dynamic system with an AMD when subjected to earthquake, as shown in figure 1, can be described as

$$\mathbf{M}_{ss}\ddot{\mathbf{x}}_{ss}(t) + \mathbf{C}_{ss}\dot{\mathbf{x}}_{ss}(t) + \mathbf{K}_{ss}\mathbf{x}_{ss}(t) = -\mathbf{M}_{ss}\mathbf{I}\ddot{x}_{\mathrm{g}}(t) + \mathbf{E}_u F(t), \tag{1}$$

where $\mathbf{x}_{ss}$ is the $n \times 1$ displacement vector of the structure relative to the ground, $\mathbf{M}_{ss}$, $\mathbf{C}_{ss}$ and $\mathbf{K}_{ss}$ are respectively the $n \times n$ mass, damping and stiffness matrices of the structure, $\mathbf{I}$ is the $n \times 1$ identity vector, $\ddot{x}_{\mathrm{g}}$ is the acceleration of the ground, $F(t)$ is the control force applied to the structure by the AMD system, and $\mathbf{E}_u$ is the $n \times 1$ AMD position vector.

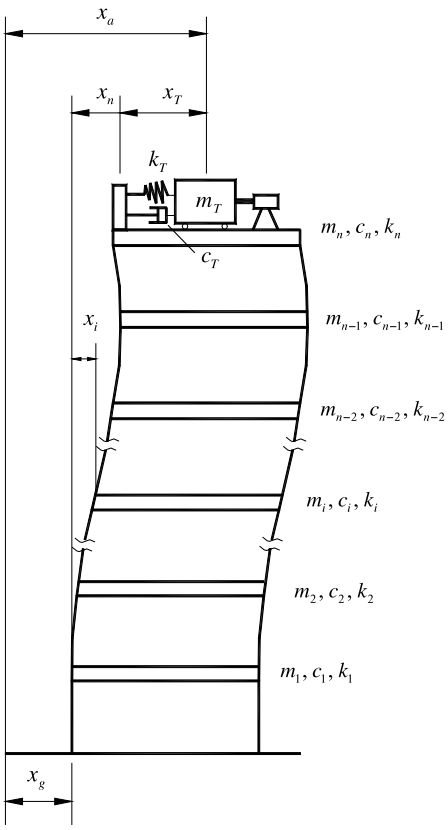

Figure 1. Sketch of structure with an AMD.

Similarly, the equation of motion of the AMD can be expressed by

$$m_{\mathrm{T}}\ddot{x}_{\mathrm{a}}(t) + c_{\mathrm{T}}\dot{x}_{\mathrm{T}}(t) + k_{\mathrm{T}}x_{\mathrm{T}}(t) = u(t), \tag{2}$$

where x_{T} is the displacement of the AMD relative to the top story, m_{T}, c_{T} and k_{T} are the mass, damping and stiffness matrices of the AMD, respectively, $u(t)$ is the force generated by the actuator, and $\ddot{x}_{\mathrm{a}}$ is the absolute acceleration of the AMD, denoted by

$$\ddot{x}_{\mathrm{a}} = \ddot{x}_{\mathrm{T}} + \ddot{x}_n + \ddot{x}_{\mathrm{g}}, \tag{3}$$

where $\ddot{x}_n$ is the acceleration of floor where the AMD is installed.

The control force $F(t)$ applied to the structure by the AMD can be described as

$$F(t) = k_{\mathrm{T}}x_{\mathrm{T}}(t) + c_{\mathrm{T}}\dot{x}_{\mathrm{T}}(t) - u(t) = -m_{\mathrm{T}}\ddot{x}_{\mathrm{a}}. \tag{4}$$

Combining equations (1) and (4) yields the dynamical model of the control system:

$$\mathbf{M}_s\ddot{\mathbf{X}}_s + \mathbf{C}_s\dot{\mathbf{X}}_s + \mathbf{K}_s\mathbf{X}_s = -\mathbf{M}_s\mathbf{E}_{\mathrm{x}}\ddot{x}_{\mathrm{g}}(t) + \mathbf{E}_{\mathrm{F}}u(t), \tag{5}$$

where

$$\mathbf{M}_s = \begin{bmatrix} m_1 & & & & \\ & m_2 & & & \\ & & \ddots & & \\ & & & m_n + m_{\mathrm{T}} & m_{\mathrm{T}} \\ & & & m_{\mathrm{T}} & m_{\mathrm{T}} \end{bmatrix}_{(n+1)\times(n+1)},$$

$$\mathbf{K}_s = \begin{bmatrix} k_1+k_2 & -k_2 & 0 & \cdots & 0 \\ -k_2 & k_2+k_3 & -k_3 & \cdots & 0 \\ & \cdots & \ddots & & \vdots \\ 0 & \cdots & -k_{n-1} & k_n & 0 \\ 0 & \cdots & \cdots & 0 & k_{\mathrm{T}} \end{bmatrix}_{(n+1)\times(n+1)}$$

and

$$\mathbf{C}_s = \begin{bmatrix} c_1+c_2 & -c_2 & 0 & \cdots & 0 \\ -c_2 & c_2+c_3 & -c_3 & \cdots & 0 \\ & \cdots & \ddots & & \vdots \\ 0 & \cdots & -c_{n-1} & c_n & 0 \\ 0 & \cdots & \cdots & 0 & c_{\mathrm{T}} \end{bmatrix}_{(n+1)\times(n+1)},$$

$$\mathbf{E}_x = \begin{bmatrix} 1 \\ \vdots \\ \vdots \\ 1 \\ 0 \end{bmatrix}_{(n+1)\times 1}, \qquad \mathbf{E}_F = \begin{bmatrix} 0 \\ \vdots \\ \vdots \\ 0 \\ 1 \end{bmatrix}_{(n+1)\times 1},$$

$$\mathbf{X}_s = \begin{bmatrix} \mathbf{x}_{ss} \\ x_{\mathrm{T}} \end{bmatrix}_{(n+1)\times 1},$$

where m_i, c_i and k_i $(i = 1, 2, \ldots, n)$ are the mass, damping and stiffness coefficients of ith story.

3. Modeling of AMD control systems with uncertainties

A mathematical model of any real system is always just an approximation of the true, physical reality of the system dynamics. Typical sources of discrepancies include unmodeled dynamics, neglected nonlinearities, effects of deliberate reduced order modes, and system parameter variations due to environmental changes and torn-and-worn factors. These modeling errors may adversely affect the performance of a control system. In this paper, we consider structural uncertainties in the control design so that robustness to these uncertainties can be ensured. The linear fractional transformation (LFT) is first introduced to model uncertainties (Zhou *et al* 1996).

The general framework of LFT is shown in figure 1. The interconnection transfer function matrix $\mathbf{M}_\Delta$ in figure 1 is partitioned as

$$\mathbf{M}_\Delta = \begin{bmatrix} \mathbf{M}_{11} & \mathbf{M}_{12} \\ \mathbf{M}_{21} & \mathbf{M}_{22} \end{bmatrix}, \tag{6}$$

where the dimensions of $\mathbf{M}_{11}$ conform with those of Δ. If ($\mathbf{I}$-$\mathbf{M}_{11}\Delta$) is invertible, it can be derived by routine manipulations so that

$$z = [\mathbf{M}_{22} + \mathbf{M}_{21}\boldsymbol{\Delta}(\mathbf{I} - \mathbf{M}_{11}\boldsymbol{\Delta})^{-1}\mathbf{M}_{12}]w. \tag{7}$$

When an inverse exists, the linear fractional transformation of $\mathbf{M}_\Delta$ and Δ is defined as

$$F_U(\mathbf{M}, \boldsymbol{\Delta}) = \mathbf{M}_{22} + \mathbf{M}_{21}\boldsymbol{\Delta}(\mathbf{I} - \mathbf{M}_{11}\boldsymbol{\Delta})^{-1}\mathbf{M}_{12}. \tag{8}$$

Since the upper loop of M is closed by the block Δ, this kind of linear fractional transformation is also called an upper linear fractional transformation and is denoted with a subscript 'U' (i.e. $F_U(\mathbf{M}, \boldsymbol{\Delta})$). With the introduction of linear fractional transformations, the uncertainties in the system can be uniformly described by figure 2 with an appropriately defined interconnection matrix.

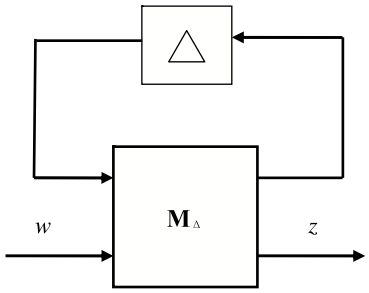

Figure 2. Standard M-Δ configuration.

In a realistic AMD control system, the physical parameters of $\mathbf{M}_s$, $\mathbf{C}_s$ and $\mathbf{K}_s$ in equation (5) are not known exactly. However, it can be assumed that their values are within certain, known intervals. That is,

$$\begin{aligned} \mathbf{M}_s &= \bar{\mathbf{M}} + \mathbf{P}_M\boldsymbol{\delta}_M\bar{\mathbf{M}} = (\mathbf{I} + \mathbf{P}_M\boldsymbol{\delta}_M)\bar{\mathbf{M}} \\ \mathbf{C}_s &= \bar{\mathbf{C}} + \mathbf{P}_C\boldsymbol{\delta}_C\bar{\mathbf{C}} = (\mathbf{I} + \mathbf{P}_C\boldsymbol{\delta}_C)\bar{\mathbf{C}} \\ \mathbf{K}_s &= \bar{\mathbf{K}} + \mathbf{P}_K\boldsymbol{\delta}_K\bar{\mathbf{K}} = (\mathbf{I} + \mathbf{P}_K\boldsymbol{\delta}_K)\bar{\mathbf{K}}, \end{aligned} \tag{9}$$

where $\bar{\mathbf{M}}$, $\bar{\mathbf{C}}$ and $\bar{\mathbf{K}}$ are the nominal values of $\mathbf{M}_s$, $\mathbf{C}_s$ and $\mathbf{K}_s$. $\boldsymbol{\delta}_M$, $\boldsymbol{\delta}_C$ and $\boldsymbol{\delta}_K$, respectively, represent the possible perturbations on those parameters. $\mathbf{P}_M$, $\mathbf{P}_C$ and $\mathbf{P}_K$ represent the maximum discrepancy between the actual system and the mathematical model. The matrices $\boldsymbol{\delta}_M$, $\boldsymbol{\delta}_C$ and $\boldsymbol{\delta}_K$ are diagonal with uncertain values. However, their values belong to $[-1, 1]$. $\mathbf{I}$ is the identity matrix.

We note that $\mathbf{M}_s^{-1}$ can be represented as an LFT in $\boldsymbol{\delta}_M$:

$$\begin{aligned} \mathbf{M}_s^{-1} &= [(\mathbf{I} + \mathbf{P}_M\boldsymbol{\delta}_M)\bar{\mathbf{M}}]^{-1} = \bar{\mathbf{M}}^{-1}[(\mathbf{I} + \mathbf{P}_M\boldsymbol{\delta}_M) \\ &\quad - \mathbf{P}_M\boldsymbol{\delta}_M](\mathbf{I} + \mathbf{P}_M\boldsymbol{\delta}_M)^{-1} \\ &= \bar{\mathbf{M}}^{-1} - \bar{\mathbf{M}}^{-1}\mathbf{P}_M\boldsymbol{\delta}_M(\mathbf{I} + \mathbf{P}_M\boldsymbol{\delta}_M)^{-1}\mathbf{I} \\ &= F_U(\mathbf{M}_M, \boldsymbol{\delta}_M) \end{aligned} \tag{10}$$

with

$$\mathbf{M}_M = \begin{bmatrix} -\mathbf{P}_M & \mathbf{I} \\ -\bar{\mathbf{M}}^{-1}\mathbf{P}_M & \bar{\mathbf{M}}^{-1} \end{bmatrix}.$$

Similarly, the parameter $\mathbf{C}_s = (\mathbf{I} + \mathbf{P}_C\boldsymbol{\delta}_C)\bar{\mathbf{C}}$ may be represented as an upper LFT in $\boldsymbol{\delta}_C$:

$$\mathbf{C}_s = F_U(\mathbf{M}_C, \boldsymbol{\delta}_C) \tag{11}$$

with

$$\mathbf{M}_C = \begin{bmatrix} \mathbf{0} & \bar{\mathbf{C}} \\ \mathbf{P}_C & \bar{\mathbf{C}} \end{bmatrix},$$

and the parameter $\mathbf{K}_s = (\mathbf{I} + \mathbf{P}_K\boldsymbol{\delta}_K)\bar{\mathbf{K}}$ may be represented as an upper LFT in $\boldsymbol{\delta}_K$:

$$\mathbf{K}_s = F_U(\mathbf{M}_K, \boldsymbol{\delta}_K) \tag{12}$$

with

$$\mathbf{M}_K = \begin{bmatrix} \mathbf{0} & \bar{\mathbf{K}} \\ \mathbf{P}_K & \bar{\mathbf{K}} \end{bmatrix}.$$

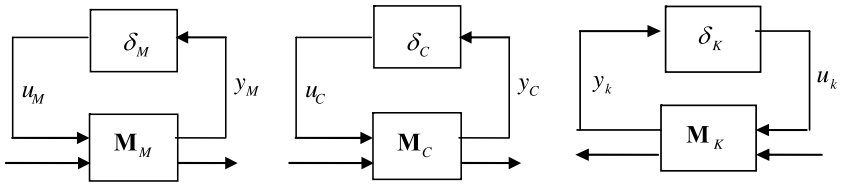

Figure 3. Representation of uncertain parameters as LFTs.

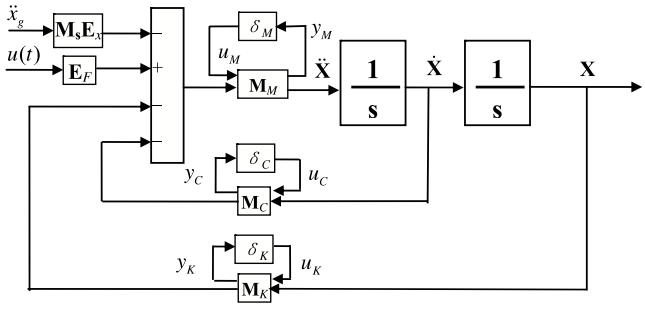

Figure 4. Block diagram of the control system with uncertainties.

To further represent the system model as an LFT of the unknown, real perturbations δ_M, δ_C and δ_K, we use the block diagrams in figure 3 and denote the inputs and outputs of δ_M, δ_C and δ_K as y_M, y_C, y_K and u_M, u_C and u_K, respectively, as shown in figure 4 (Gu *et al* 2005).

Let the state variable be $[\mathbf{X}_s^{\mathrm{T}}\ \dot{\mathbf{X}}_s^{\mathrm{T}}]^{\mathrm{T}}$ and the measurement y be the absolute acceleration of structures. The governing equations of the system dynamics are given by

$$\begin{bmatrix} \dot{X}_S \\ \ddot{X}_s \\ \cdots \\ y_M \\ y_C \\ y_K \\ \cdots \\ y \end{bmatrix} = \left[\begin{array}{ccccc} A & \vdots & B_1 & B_2 \\ \cdots & \cdots & \cdots & \cdots \\ C_1 & \vdots & D_{11} & D_{12} \\ C_2 & \vdots & D_{21} & D_{22} \end{array}\right] \begin{bmatrix} X_S \\ \dot{X}_S \\ \cdots \\ u_M \\ u_C \\ u_K \\ \cdots \\ \dot{x}_{\mathrm{g}} \\ u \end{bmatrix}. \quad (13)$$

Therefore, the input/output dynamics of the control system that takes into account the uncertainty of parameters can be denoted by G, as shown in figure 5. The state space representation of G is

$$G = \left[\begin{array}{c|cc} A & B_1 & B_2 \\ \hline C_1 & D_{11} & D_{12} \\ C_2 & D_{21} & D_{22} \end{array}\right], \quad (14)$$

where

$$\mathbf{A} = \begin{bmatrix} \mathbf{0} & \mathbf{I} \\ -\bar{\mathbf{M}}^{-1}\bar{\mathbf{K}} & -\bar{\mathbf{M}}^{-1}\bar{\mathbf{C}} \end{bmatrix},$$

$$\mathbf{B_1} = \begin{bmatrix} \mathbf{0} & \mathbf{0} & \mathbf{0} \\ -\bar{\mathbf{M}}^{-1}\mathbf{P}_{\mathrm{M}} & -\bar{\mathbf{M}}^{-1}\mathbf{P}_{\mathrm{C}} & -\bar{\mathbf{M}}^{-1}\mathbf{P}_{\mathrm{K}} \end{bmatrix},$$

$$\mathbf{B_2} = \begin{bmatrix} \mathbf{0} & \mathbf{0} \\ -\mathbf{E}_x & \bar{\mathbf{M}}^{-1}\mathbf{E}_{\mathrm{F}} \end{bmatrix},$$

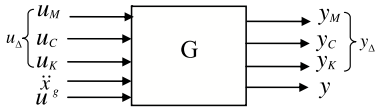

Figure 5. Input/output block diagram of the system.

$$\mathbf{C_1} = \begin{bmatrix} -\bar{\mathbf{M}}^{-1}\bar{\mathbf{C}} & -\bar{\mathbf{M}}^{-1}\bar{\mathbf{K}} \\ \mathbf{0} & \bar{\mathbf{C}} \\ \bar{\mathbf{K}} & \mathbf{0} \end{bmatrix},$$

$$\mathbf{D_{11}} = \begin{bmatrix} -\bar{\mathbf{M}}^{-1}\mathbf{P}_{\mathrm{M}} & -\bar{\mathbf{M}}^{-1}\mathbf{P}_{\mathrm{C}} & -\bar{\mathbf{M}}^{-1}\mathbf{P}_{\mathrm{K}} \\ \mathbf{0} & \mathbf{0} & \mathbf{0} \\ \mathbf{0} & \mathbf{0} & \mathbf{0} \end{bmatrix},$$

$$\mathbf{D_{12}} = \begin{bmatrix} -\mathbf{E}_{\mathrm{x}} & \mathbf{M}^{-1}\mathbf{E}_{\mathrm{F}} \\ \mathbf{0} & \mathbf{0} \\ \mathbf{0} & \mathbf{0} \end{bmatrix},$$

$$\mathbf{C_2} = [\, -\mathbf{D}_{\mathrm{y}}\bar{\mathbf{M}}^{-1}\bar{\mathbf{K}} \quad -\mathbf{D}_{\mathrm{y}}\bar{\mathbf{M}}^{-1}\bar{\mathbf{C}} \,],$$

$$\mathbf{D_{21}} = [\, -\mathbf{D}_{\mathrm{y}}\bar{\mathbf{M}}^{-1}\mathbf{P}_{\mathrm{M}} \quad -\mathbf{D}_{\mathrm{y}}\mathbf{M}^{-1}\mathbf{P}_{\mathrm{C}} \quad -\mathbf{D}_{\mathrm{y}}\bar{\mathbf{M}}^{-1}\mathbf{P}_{\mathrm{K}} \,],$$

$$\mathbf{D_{22}} = [\, \mathbf{0} \quad \mathbf{D}_{\mathrm{y}}\bar{\mathbf{M}}^{-1}\mathbf{E}_{\mathrm{F}} \,],$$

where $\mathbf{D}_{\mathrm{y}}$ denotes the position vector of the accelerometers.

Let $\Delta = \mathrm{diag}(\delta_M, \delta_C, \delta_K)$, $u_\Delta = [u_M, u_C, u_K]$ and $y_\Delta = [y_M, y_C, y_K]$. Then, the effects of uncertain structural parameters on the system G can be expressed by

$$u_\Delta = \Delta \cdot y_\Delta. \quad (15)$$

4. Formulation of the LMI based H_∞ control for an AMD-structure system

In this section, we will transform the computation of an optimal controller for the AMD-structure system into a general H_∞ control frame. Weighting functions are used to adjust the system's performance. The advantages of using weighted functions are obvious in controller design (Zhou *et al* 1996). First, some components of a vector signal are usually more important than others. Second, each component of the signal may not be measured in the same units. For example, in the AMD control problem shown in figure 5, the input is a voltage signal and the output y is measured in terms of acceleration. Also, we might be primarily interested in rejecting errors in a certain frequency range. Therefore, frequency-dependent weights must be chosen to obtain a high performance controller (Zhou *et al* 1996).

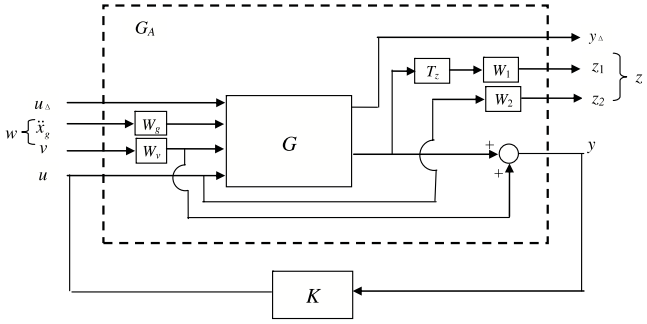

Figure 6. A typical control block diagram for a seismically excited structure.

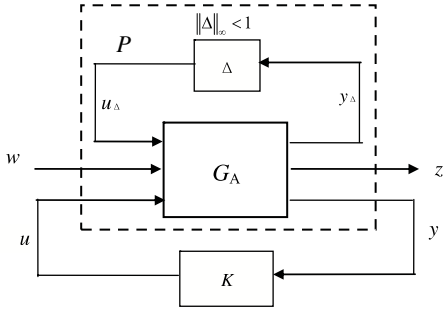

Figure 7. General robust control scheme.

A detailed block diagram representation of the system is depicted in figure 6. The frequency domain weighted function W_g shapes the spectral content of the disturbance modeling the earthquake excitation. W_v is used to weight the measurement noise v. The block T_z is a constant matrix that dictates the regulated response transformed from the measurement vector. The matrix weighting functions W_1 and W_2 are frequency dependent, with W_1 weighting regulated response and W_2 weighting the control signal. K is the controller that generates a control signal u according to the measured response y. The input excitation w consists of earthquake excitation $\ddot{x}_g$ and measurement noise v. The output z comprises the frequency weighted regulated response and control signal. The regulated response denotes the quantities of the design interest that can be floor acceleration, floor displacement or base shear force, etc. The rectangle denoted with a dashed line in figure 6 represents the augmented system model G_A.

H_∞ control methods provide controllers with robustness to external disturbances and system parameter uncertainties, such as modeling errors and system parameter perturbations. Therefore, these controllers can guarantee stability and optimized vibration suppression performance despite imprecise or inaccurate knowledge of the structural system parameters. The formulations of the H_∞ control problem in terms of linear matrix inequalities (LMIs), which allows computationally efficient and systematic design of robust controllers (Skelton *et al* 1998), is used here. Using the LFT, the vibration control of structures with AMDs can be represented by a general block diagram, as shown in figure 7, and is expressed by

$$\begin{aligned} \dot{\mathbf{x}}_P &= \mathbf{A}_P\mathbf{x}_P + \mathbf{B}_P\mathbf{u} + \mathbf{D}_P\mathbf{w} \\ \mathbf{z} &= \mathbf{C}_z\mathbf{x}_P + \mathbf{B}_z\mathbf{u} + \mathbf{D}_z\mathbf{w} \\ \mathbf{y} &= \mathbf{C}_y\mathbf{x}_P + \mathbf{D}_y\mathbf{w}, \end{aligned} \tag{16}$$

where $\mathbf{x}_P$ is the state variable of the augmented system model P. Let the transfer matrix from w to z be denoted by T_{zw}. The H_∞ norm of the control system is defined as $\|T_{zw}\|_\infty = \sup_w \bar{\sigma}(T_{zw}(\mathrm{j}\omega))$ and the H_∞ control problem here is to design a controller K to make the closed-loop system stable and $\|T_{zw}\|_\infty$ minimal. The LMI formulation of the H_∞ control problem results in an efficient optimization method that can handle large-scale systems. LMI optimization problems are convex, leading to computationally efficient global optimal solutions (Bai 2006, Bai *et al* 2007).

Consider a system with order n_c that has the state space representation of (16). The following formulation is useful in designing a controller K of order n_K that is less than or equal to n_c with the following state space representation:

$$\begin{aligned} \dot{\mathbf{x}}_c &= \mathbf{A}_c\mathbf{x}_c + \mathbf{B}_c\mathbf{y} \\ \mathbf{u} &= \mathbf{C}_c\mathbf{x}_c + \mathbf{D}_c\mathbf{y}, \end{aligned} \tag{17}$$

where x_c is the state vector of controller, u is the control signal, y is the output of the generalized plant shown in equation (16), and $\mathbf{A}_c$, $\mathbf{B}_c$, $\mathbf{C}_c$ and $\mathbf{D}_c$ are real matrices of appropriate dimensions.

Assembling the equations (16) and (17) yields

$$\begin{aligned} \begin{bmatrix} \dot{\mathbf{x}}_P(\mathbf{t}) \\ \dot{\mathbf{x}}_c(\mathbf{t}) \end{bmatrix} &= \begin{bmatrix} \mathbf{A}_P + \mathbf{B}_P\mathbf{D}_c\mathbf{C}_y & \mathbf{B}_P\mathbf{C}_c \\ \mathbf{B}_c\mathbf{C}_y & \mathbf{A}_c \end{bmatrix} \begin{bmatrix} \mathbf{x}_P \\ \mathbf{x}_c \end{bmatrix} \\ &\quad + \begin{bmatrix} \mathbf{B}_P\mathbf{D}_c\mathbf{D}_y + \mathbf{D}_P \\ \mathbf{B}_c\mathbf{D}_y \end{bmatrix} \mathbf{w} \\ \mathbf{z} &= [\,\mathbf{C}_z + \mathbf{B}_z\mathbf{D}_c\mathbf{C}_y \quad \mathbf{B}_z\mathbf{C}_c\,] \begin{bmatrix} \mathbf{x}_P \\ \mathbf{x}_c \end{bmatrix} + \left[\mathbf{B}_z\mathbf{D}_c\mathbf{D}_y + \mathbf{D}_z\right]\mathbf{w}, \end{aligned} \tag{18}$$

or simply

$$\begin{aligned} \dot{\mathbf{x}}(t) &= \mathbf{A}_{cl}\mathbf{x}(t) + \mathbf{B}_{cl}\mathbf{w}(t) \\ \mathbf{z}(t) &= \mathbf{C}_{cl}\mathbf{x}(t) + \mathbf{D}_{cl}\mathbf{w}(t), \end{aligned} \tag{19}$$

where

$$\mathbf{A}_{cl} = \mathbf{A}_l + \mathbf{B}_l\mathbf{K}\mathbf{M}, \qquad \mathbf{B}_{cl} = \mathbf{D}_l + \mathbf{B}_l\mathbf{K}\mathbf{E},$$

$$\mathbf{C}_{cl} = \mathbf{C}_l + \mathbf{H}\mathbf{K}\mathbf{M}, \qquad \mathbf{D}_{cl} = \mathbf{F} + \mathbf{H}\mathbf{K}\mathbf{E}$$

$$\mathbf{A}_l = \begin{bmatrix} \mathbf{A}_P & \mathbf{0} \\ \mathbf{0} & \mathbf{0} \end{bmatrix}, \qquad \mathbf{B}_l = \begin{bmatrix} \mathbf{B}_P & \mathbf{0} \\ \mathbf{0} & \mathbf{I} \end{bmatrix},$$

$$\mathbf{K} = \begin{bmatrix} \mathbf{D}_c & \mathbf{C}_c \\ \mathbf{B}_c & \mathbf{A}_c \end{bmatrix}, \qquad \mathbf{M} = \begin{bmatrix} \mathbf{C}_y & \mathbf{0} \\ \mathbf{0} & \mathbf{I} \end{bmatrix},$$

$$\mathbf{D}_l = \begin{bmatrix} \mathbf{D}_P \\ \mathbf{0} \end{bmatrix}, \qquad \mathbf{E} = \begin{bmatrix} \mathbf{D}_y \\ \mathbf{0} \end{bmatrix},$$

$$\mathbf{C}_l = [\,\mathbf{C}_z \quad \mathbf{0}\,], \qquad \mathbf{H} = [\,\mathbf{B}_z \quad \mathbf{0}\,], \qquad \mathbf{F} = \mathbf{D}_z.$$

The notation to be used is as follows: given a real matrix N, the orthogonal complement $N^\perp$ is defined as the (possibly non-unique) matrix with a maximum row rank that satisfies $N^\perp N = 0$ and $N^\perp N^\perp > 0$. Hence, $N^\perp$ can be computed from the singular value decomposition of N as follows: $N^\perp =$

TU_2^{T}, where T is an arbitrary nonsingular matrix and U_2 is defined from the singular value decomposition of N:

$$N = [\,U_1 \quad U_2\,]\begin{bmatrix}\sum_1 & 0\\ 0 & 0\end{bmatrix}\begin{bmatrix}V_1^{\mathrm{T}}\\ V_2^{\mathrm{T}}\end{bmatrix}. \tag{20}$$

The standard notation $>$ ($<$) is used to denote the positive (negative) definite ordering of symmetric matrices. The ith eigenvalue of a real symmetric matrix N is denoted by $\lambda_i(N)$, where the ordering of the eigenvalues is defined as $\lambda_{\max}(N) = \lambda_1(N) \geqslant \lambda_2(N) \geqslant \cdots \geqslant \lambda_n(N)$. The maximum singular value of a (not necessarily square) matrix N is denoted by $\sigma_{\max}(N)$, which is also its spectral norm $\|N\|$. N^+ denotes the Moore–Penrose generalized inverse of a matrix N (Skelton *et al* 1998).

To design an H_∞ controller using LMI for a system expressed by equation (18), one must find a matrix pair $(\mathbf{X}_P, \mathbf{Y}_P)$ with dimension of $n_P \times n_P$ such that the following statements are satisfied for a given scalar $\gamma > 0$:

$$\begin{bmatrix}\mathbf{X}_P & \gamma\mathbf{I}\\ \gamma\mathbf{I} & \mathbf{Y}_P\end{bmatrix} \geqslant 0, \qquad \operatorname{rank}\begin{bmatrix}\mathbf{X}_P & \gamma\mathbf{I}\\ \gamma\mathbf{I} & \mathbf{Y}_P\end{bmatrix} \leqslant n_P + n_c \tag{21}$$

$$\begin{bmatrix}\mathbf{B}_P\\ \mathbf{B}_z\end{bmatrix}^{\perp}\begin{bmatrix}\mathbf{A}_P\mathbf{X}_P + \mathbf{X}_P\mathbf{A}_P^{\mathrm{T}} + \mathbf{D}_P\mathbf{D}_P^{\mathrm{T}} & \mathbf{X}_P\mathbf{C}_P^{\mathrm{T}} + \mathbf{D}_P\mathbf{D}_z^{\mathrm{T}}\\ \mathbf{C}_P\mathbf{X}_P + \mathbf{D}_z\mathbf{D}_P^{\mathrm{T}} & \mathbf{D}_z\mathbf{D}_z^{\mathrm{T}} - \gamma^2\mathbf{I}\end{bmatrix} \times \begin{bmatrix}\mathbf{B}_P\\ \mathbf{B}_z\end{bmatrix}^{\perp T} < 0 \tag{22}$$

$$\begin{bmatrix}\mathbf{C}_y^{\mathrm{T}}\\ \mathbf{D}_y^{\mathrm{T}}\end{bmatrix}^{\perp}\begin{bmatrix}\mathbf{Y}_P\mathbf{A}_P + \mathbf{A}_P^{\mathrm{T}}\mathbf{Y}_P + \mathbf{C}_z^{\mathrm{T}}\mathbf{C}_z & \mathbf{Y}_P\mathbf{D}_P + \mathbf{C}_z^{\mathrm{T}}\mathbf{D}_z\\ \mathbf{D}_P^{\mathrm{T}}\mathbf{Y}_P + \mathbf{D}_z^{\mathrm{T}}\mathbf{C}_z & \mathbf{D}_z^{\mathrm{T}}\mathbf{D}_z - \gamma^2\mathbf{I}\end{bmatrix} \times \begin{bmatrix}\mathbf{C}_y^{\mathrm{T}}\\ \mathbf{D}_y^{\mathrm{T}}\end{bmatrix}^{\perp T} < 0. \tag{23}$$

One can compute a matrix factor $\mathbf{Y}_{pc}$ and $\mathbf{Y}_c > 0$ according to $(\mathbf{X}_P, \mathbf{Y}_P)$ such that

$$\mathbf{Y}_{pc}\mathbf{Y}_c^{-\perp}\mathbf{Y}_{pc}^{\mathrm{T}} = \mathbf{Y}_P - \gamma^2\mathbf{X}_P^{-1} \tag{24}$$

and construct $\mathbf{Y}$ and $\mathbf{X}$ as

$$\mathbf{Y} = \begin{bmatrix}\mathbf{Y}_P & \mathbf{Y}_{pc}\\ \mathbf{Y}_{pc}^{\mathrm{T}} & \mathbf{Y}_c\end{bmatrix}, \qquad \mathbf{X} = \gamma^2\mathbf{Y}^{-1}. \tag{25}$$

Then, the controller is given by

$$\mathbf{K} = -\mathbf{R}^{-1}\mathbf{\Gamma}^{\mathrm{T}}\mathbf{\Phi}\Lambda^{\mathrm{T}}(\mathbf{\Lambda}\mathbf{\Phi}\mathbf{\Lambda}^{\mathrm{T}})^{-1} + \mathbf{S}^{1/2}\mathbf{L}(\mathbf{\Lambda}\mathbf{\Phi}\mathbf{\Lambda}^{\mathrm{T}})^{-1/2}, \tag{26}$$

where $\mathbf{L}$ is an arbitrary matrix such that $\|\mathbf{L}\| < 1$, and $\mathbf{R}$ is an arbitrary positive definite matrix such that

$$\mathbf{\Phi} = (\mathbf{\Gamma}\mathbf{R}^{-1}\mathbf{\Gamma}^{\mathrm{T}} - \mathbf{\Theta})^{-1} > 0 \tag{27}$$

and

$$\mathbf{S} = \mathbf{R}^{-1} - \mathbf{R}^{-1}\mathbf{\Gamma}^{\mathrm{T}}[\mathbf{\Phi} - \mathbf{\Phi}\Lambda^{\mathrm{T}}(\mathbf{\Lambda}\mathbf{\Phi}\mathbf{\Lambda}^{\mathrm{T}})^{-1}\mathbf{\Lambda}\mathbf{\Phi}]\mathbf{\Gamma}\mathbf{R}^{-1} \tag{28}$$

$$\Theta = \begin{bmatrix}\mathbf{Y}\mathbf{A}_l + \mathbf{A}_l\mathbf{Y} & \mathbf{Y}\mathbf{D}_l & \mathbf{C}_l^{\mathrm{T}}\\ \mathbf{D}_l^{\mathrm{T}}\mathbf{A} & -\gamma^2\mathbf{I} & \mathbf{F}^{\mathrm{T}}\\ \mathbf{C}_l & \mathbf{F} & -\mathbf{I}\end{bmatrix}, \qquad \Gamma = \begin{bmatrix}\mathbf{Y}\mathbf{B}_l\\ \mathbf{0}\\ \mathbf{H}\end{bmatrix}, \qquad \Lambda = [\,\mathbf{M} \quad \mathbf{E} \quad \mathbf{0}\,]. \tag{29}$$

The proof of equations (26) can be found in Skelton *et al* (1998). This LMI based H_∞ control design will be used for active vibration suppression of a model building using an AMD.

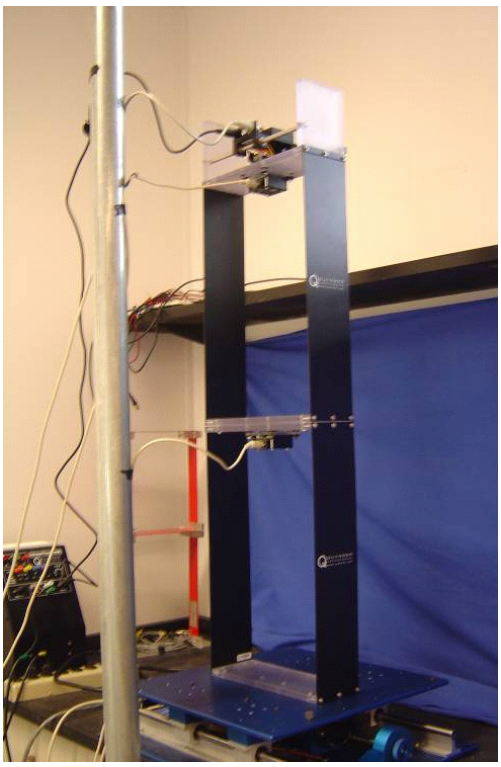

Figure 8. Photo of the experimental set-up.

5. Shaking table test of a flexible structure with an AMD

5.1. Experimental set-up

To demonstrate the effectiveness of the proposed robust H_∞ controller, shaking table tests of a small-scale two-story structure with an AMD shown in figure 8 were conducted in the Smart Materials and Smart Structures Laboratory at the University of Houston. The structural inter-story height is 490 mm. The first floor mass is 1.16 kg and the second is 1.38 kg. The structure has natural frequencies of 1.4 and 4.4 Hz. A moving cart driven by a DC motor is installed on the top of structure acting as an AMD control device. The moving cart is driven by a brushless DC motor sliding along a geared rack, which generates control forces to the structure. The maximum stroke of the AMD is $\pm$9.5 cm with a total moving mass of 0.65 kg. Each floor of the building is equipped with an accelerometer. The accelerometers are manufactured by Quanser Consulting Inc., and they produce an output of $\pm$5 V with a range of $\pm 5g$. Two universal power modules (UPMs) are used as power amplifiers; one of them is used to power the shaking table and the other one is used to power the AMD. The data acquisition and control board used to collect data and drive the power amplifier is a Q8 extended terminal board manufactured by Quanser Consulting Inc. Features of the board include an 8-channel analog-to-digital converter with an input range of $\pm$10 V, 14-bit resolution. In addition, the board contains an 8-channel digital-to-analog converter with an output range of $\pm$10 V and 12-bit resolution.

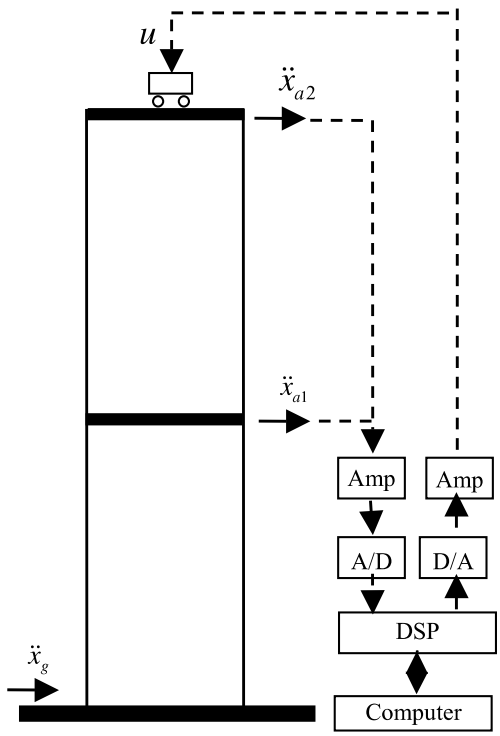

Figure 9. Scheme of an AMD control system.

A diagram of the control system is shown in figure 9. The structure is controlled by the AMD, subjected to shaking table movement excitation. The acceleration signals on both stories are used as feedback signals after amplification and passage through the A/D converter. Using the proposed controller, a control signal is produced based on the feedback signals. After passage through the D/A converter and amplification, the control signal is sent to the AMD device and it generates a control force. Operation of the shaking table involves the use of software programs including Wincon, Visual C++, Matlab, Simulink and Real-Time Workshop. Wincon is a product of Quanser Consulting Inc., and is used for real-time feedback control and digital signal processing. Matlab/Simulink is used for control system design. Specifically, Wincon converts a Simulink block diagram to controller code using the Real-Time Workshop, compiles and links the controller code using Visual C++ and runs the controller code in real time.

5.2. Controller design

To guarantee the safety of the structure, the regulated output z_1 in figure 6 is selected to be the displacement of the second floor. The weighted function W_g is used to reflect the frequency content of an earthquake. The most commonly used stochastic model of earthquakes is the Kanai–Tajimi spectrum, as shown in the following equation:

$$S(\omega) = S_0 \left[\frac{\omega_g^4 + 4\omega_g^2 \zeta_g^2 \omega^2}{(\omega^2 - \omega_g^2)^2 + 4\omega_g^2 \zeta_g^2 \omega^2} \right]. \tag{30}$$

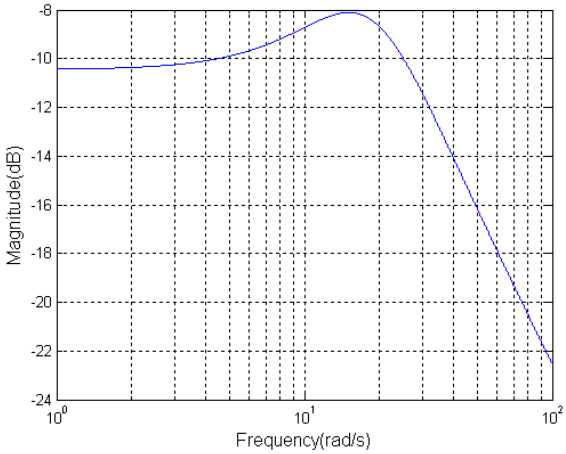

Figure 10. Frequency response of weighted function W_g.

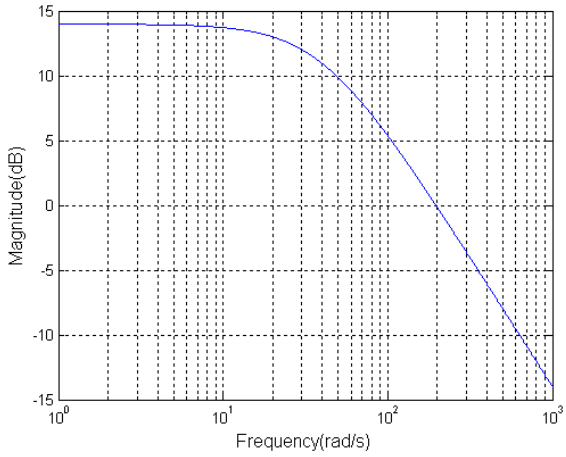

Figure 11. Frequency response of weighted function W_1.

The weighted function W_g is chosen as the square root of the Kanai–Tajimi spectrum (Spencer *et al* 1994),

$$W_g(s) = \frac{\sqrt{S_0}(\omega_g^2 + 2\zeta_g \omega_g s)}{s^2 + 2\zeta_g \omega_g s + \omega_g^2}. \tag{31}$$

The parameters of the Kanai–Tajimi spectrum used in this paper are $S_0 = 0.09$, $\zeta_g = 0.65$, and $\omega_g = 18.65$. The frequency response of W_g is shown in figure 10. For the regulated response z_1, we are only interested in the low-frequency response. Therefore, the weighted function W_1 is selected as

$$W_1(s) = \frac{5}{(1/40)s + 1} \tag{32}$$

and the frequency response is plotted in figure 11. The weighted functions W_2 and W_v are set to be 5×10^{-4} and 1, which means that the control signal and the noise are weighted in the entire frequency region. We let $\mathbf{P}_M = \text{diag}(0.1, 0.1, 0.1)$, $\mathbf{P}_C = \text{diag}(0.4, 0.4, 0.4)$ and $\mathbf{P}_K = \text{diag}(0.4, 0.4, 0.4)$. This represents up to 10% uncertainty in the mass, and 40% uncertainty in the damping and stiffness coefficients of the control system.

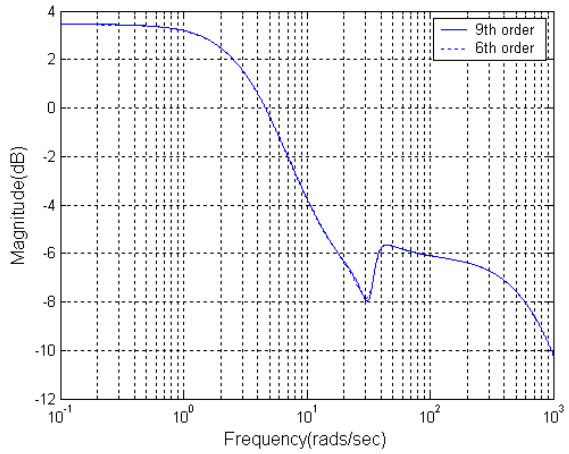

Figure 12. Frequency response of controller and reduced order controller (channel 1).

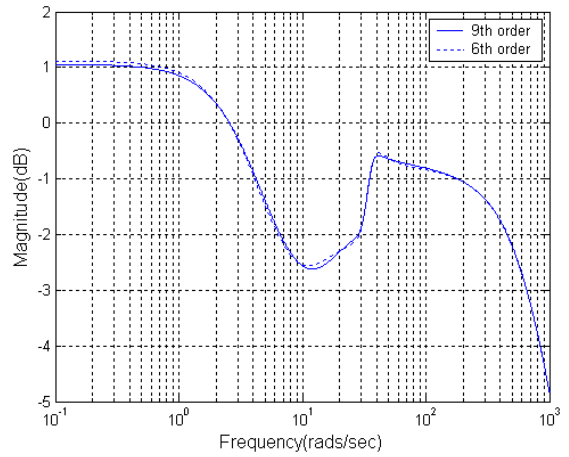

Figure 13. Frequency response of controller and reduced order controller (channel 2).

A ninth-order H_∞ controller is designed based on the LMI approach of section 4 and then reduced to a sixth-order controller using the balanced truncation method to facilitate the implementation. The controller takes the acceleration responses of the two-story structure as its two inputs. The first channel of the controller comes from the acceleration of the first floor to the actuator and the second channel comes from acceleration of the second floor to the actuator. The frequency responses of two channels for the ninth-order and sixth-order channels are shown in figures 12 and 13, respectively.

For comparison, a pole placement controller is also designed. The poles of the open-loop system are $-0.4049 + 32.3444j$, $-0.4049 - 32.3444j$, $-0.6680 + 10.6856j$, $-0.6680 - 10.6856j$, -16.54 and 0. The controller K is determined so that the closed-loop poles due to the feedback law are placed at the following locations: $-6+15j$, $-6-15j$, $-7+10j$, $-7-10j$, $-16+13j$ and $-16-13j$, to increase damping of the closed-loop system. As a result, the state-feedback K for pole placement control can be expressed as follows (Quanser Consulting Corporation 1995):

$$K = [51.85, 159.59, -501.14, 4.94, 30.67, -25.48]. \quad (33)$$

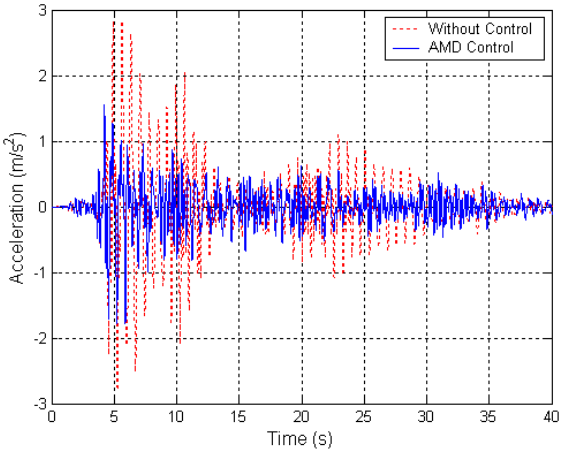

Figure 14. Acceleration history of the first floor.

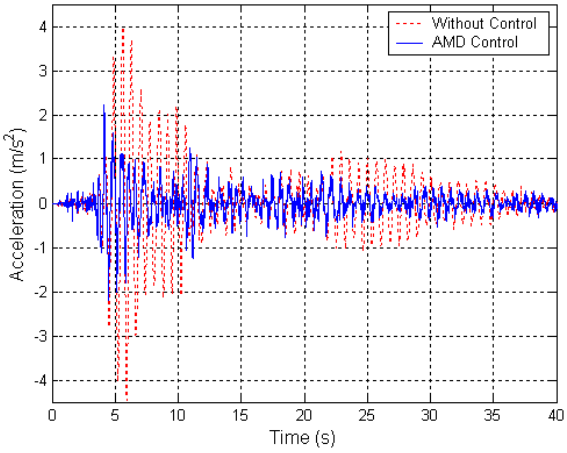

Figure 15. Acceleration history of the second floor.

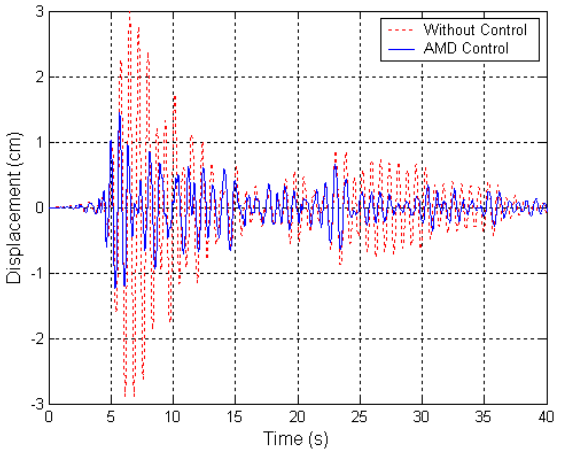

Figure 16. Displacement history of the first floor.

5.3. Experimental results

To verify the effectiveness of the designed robust H_∞ controller, shaking table tests of the two-story building model with AMD introduced previously were conducted. The

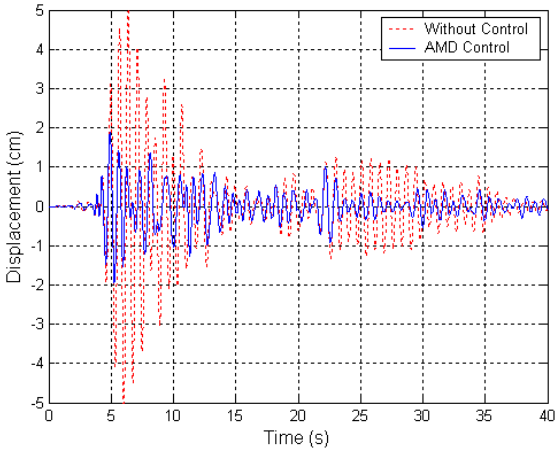

Figure 17. Displacement history of the second floor.

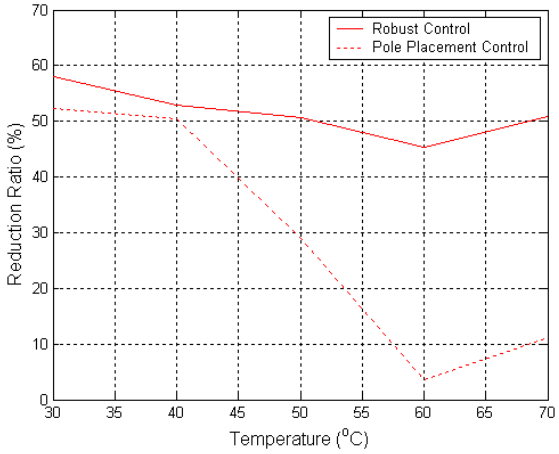

Figure 19. Displacement reduction ratio with temperature of SMA wire.

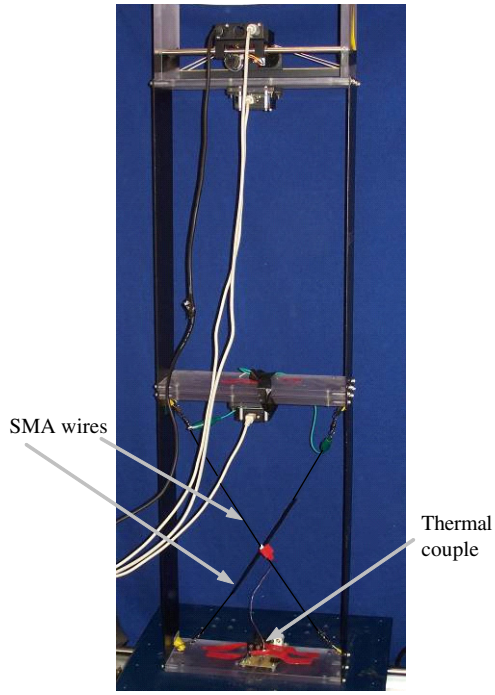

Figure 18. AMD-structure with SMA wire.

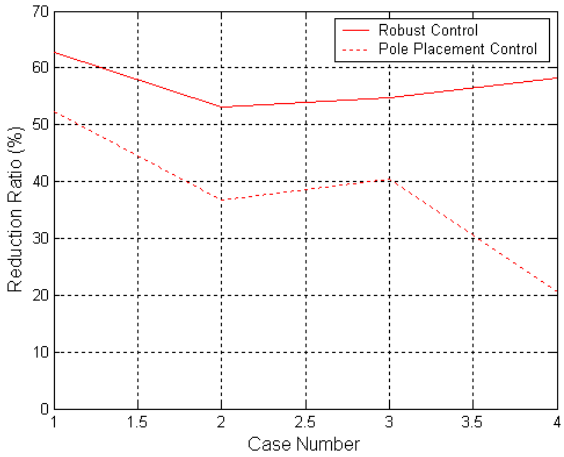

Figure 20. Displacement reduction ratio with different mass uncertainties.

El Centro earthquake record in 1940 with a peak value scaled to 0.2g was inputted to the shaking table as the excitation source. The time histories of acceleration and displacement for both stories are shown from figures 14 to 17. It can be seen from these figures that the structural responses, especially the displacements, are reduced greatly. The reduction ratios of the displacement in the first floor and second floor are 51.27% and 62.69%, respectively.

To experimentally investigate the robustness of the designed H_∞ and pole placement controllers, a diagonal shape memory alloy (SMA) wire brace was installed in the first floor to introduce stiffness uncertainty to the system by electrically hearing the SMA wire brace (as shown in figure 18). The higher the temperature of the SMA wires, the more stiffness variation is introduced to the structure. A separate PID (proportional, integral, plus derivative) controller is used to control the temperature of the SMA wires. The building model on the shaking table was excited by the same scaled El Centro earthquake with the temperature of the SMA wire held at 30, 40, 50, 60 and 70 °C. The displacement reduction ratios of the second floor for the H_∞ and pole placement controllers are shown in figure 19. Compared with the result of the pole placement controller, the reduction ratio for the H_∞ controller keeps a high value though the stiffness of the structure changes with the temperature of the SMA wire, verifying the H_∞ controller's robustness to stiffness uncertainties.

Mass uncertainties were introduced by adding additional masses on each floor. The following four cases were considered in the experiment to investigate the influence of mass uncertainties on the effectiveness of the controllers.

Case 1: Structural vibration control without additional masses.

Case 2: Structural vibration control with 1 kg (86% of the first floor mass) additional mass on the first floor.

Case 3: Structural vibration control with 1 kg (72% of the second floor mass) additional mass on the second floor.

Case 4: Structural vibration control with 0.5 kg (43% of the first and 36% of the second floor mass) additional mass on both floors.

The building test-bed on the shaking table was again excited by the scaled El Centro earthquake signal, and the reduction ratios of the second floor displacement for the four different cases are shown in figure 20. Compared with the results of the pole placement controller, the reduction ratio for the H_∞ controller is nearly unchanged despite the structural mass being dramatically changed, verifying the robustness of the designed H_∞ controller to mass uncertainties.

6. Conclusions

The mathematical model of a civil engineering structure is always an approximation of the true, physical reality of the system dynamics. Therefore, one important issue in designing reliable active control systems for civil structures is the robustness of the controller. This paper outlines a general approach toward the design of an H_∞ controller for structural vibration suppression using an active mass damper (AMD) with structural uncertainties. The system uncertainties are taken into account by the linear fractional transformation (LFT) approach. To facilitate the computation of the H_∞ controller, an efficient solution procedure based on linear matrix inequalities (LMIs) is employed. An H_∞ controller is designed for a two-story building test-bed with an AMD using the LMI method that utilizes the acceleration signals as feedback. Shaking table tests of the two-story building model were conducted with the 1940 El Centro earthquake record as the excitation source. The results show that the structural responses are reduced significantly with the proposed controller. The robustness of the designed control is also investigated by introducing stiffness and mass uncertainties to the building model. Stiffness uncertainties were introduced by installing a pair of diagonal shape memory alloy (SMA) wire braces in the first floor. When the SMA wire is heated the stiffness of the structure is perturbed. Mass uncertainties were introduced by adding additional masses to the structure. The results of the H_∞ controller were compared with those of a pole placement controller. The results show that the displacement reduction ratio of the second floor was kept at a high level with the changes of structural stiffness and mass in the case of the designed H_∞ controller, while the ratio dramatically decreased in the case of the pole placement controller. The experiment results demonstrate the effectiveness of the designed H_∞ controller in actively suppressing structural vibrations, and more importantly, the robustness of the H_∞ controller to structural stiffness and mass variations.

Acknowledgments

The second author (G Song) would like to thank the National Science Foundation of USA for the financial support of the reported research via a CAREER AWARD (No. 0305027). Any opinions, findings, and conclusions or recommendations expressed in this material are those of the author(s) and do not necessarily reflect the views of the sponsor.

References

Bai Y 2006 Advanced controls of large scale structural systems using linear matrix inequality methods *PhD Dissertation* University of Houston

Bai Y, Grigoriadis K and Song G 2007 Active fault-tolerant control of a flexible beam *Proc. 2007 SPIE Int. Symp. on Smart Structures and Materials* **6523** 65230K

Chen J and Patton R J 1999 *Robust Model-Based Fault Diagnosis for Dynamic Systems* (Norwell, MA: Kluwer–Academic)

Doyle J C, Glover K, Khargonekar P P and Francis B A 1989 State–space solutions to standard H_2 and H_∞ control problems *IEEE Trans. Autom. Control* **34** 831–47

Gahinet P and Apkarian P 1994 A linear matrix inequality approach to H_∞ control *Int. J. Robust Nonlinear Control* **4** 421–48

Gu D-W, Petkov P H and Konstantinov M M 2005 *Robust Control Design with Matlab* (London: Springer)

Housner G W, Bergman L A, Caughey T K, Chassiakos A G, Claus R O, Masri S F, Skelton R E, Spencer B F and Yao J T P 1997 Structural control: past, present, and future *J. Eng. Mech. ASCE* **123** 897–971

Iwasaki T and Skelton R E 1994 All controllers for the general H_∞ control problem: LMI existence conditions and state space formulas *Automatica* **30** 1307–17

Kobori T, Koshiak N, Yamada K and Ikeda Y 1991 Seismic response controlled structure with active mass driver system—part 1 *Earthquake Eng. Struct. Dyn.* **20** 133–49

Kwakernaak H 1993 Robust control and H_∞ optimization: tutorial paper *Automatica* **29** 255–73

Quanser Consulting Corporation 1995 *User Manuals* Ontario, Canada

Skelton R E, Iwasaki T and Grigoriadis K M 1998 *A Unified Algebraic Approach to Linear Control Design* (London: Taylor and Francis)

Spencer B F, Suhardjo J and Sain M K 1994 Frequency domain optimal control strategies for a seismic protection *J. Eng. Mech.* **120** 135–58

Wang S-G, Lin S, Shieh L S and Sunkel J W 1998 Observer based controller for robust pole clustering in a vertical strip and disturbance rejection in structured uncertain systems *Int. J. Robust Nonlinear Control* **8** 1073–84

Wang S-G, Shieh L S and Sunkel J W 1995a Robust optimal pole-clustering in a vertical strip and disturbance rejection for Lagrange's systems *Int. J. Dyn. Control* **5** 295–312

Wang S-G, Shieh L S and Sunkel J W 1995b Robust optimal pole-placement in a vertical strip and disturbance rejection *Int. J. Syst. Sci.* **26** 1839–53

Zhou K, Doyle J C and Glover K 1996 *Robust and Optimal Control* (Upper Saddle River, NJ: Prentice-Hall)